



# Higher-dimensional exceptional points and peakon dynamics triggered by spatially varying Kerr nonlinear media and $\mathcal{PT}$ $\delta(x)$ potentials

Yong Chen <sup>1</sup>, Zhenya Yan <sup>2,3,\*</sup> and Dumitru Mihalache <sup>4</sup>

<sup>1</sup>*School of Mathematics and Statistics, Jiangsu Normal University, Xuzhou 221116, China*

<sup>2</sup>*KLMM, Academy of Mathematics and Systems Science, Chinese Academy of Sciences, Beijing 100190, China*

<sup>3</sup>*School of Mathematical Sciences, University of Chinese Academy of Sciences, Beijing 100049, China*

<sup>4</sup>*Horia Hulubei National Institute of Physics and Nuclear Engineering, 077125 Magurele, Bucharest, Romania*



(Received 2 February 2023; accepted 16 November 2023; published 11 December 2023)

Higher-dimensional  $\mathcal{PT}$ -symmetric potentials constituted by delta-sign-exponential (DSE) functions are created in order to show that the exceptional points in the non-Hermitian Hamiltonian can be converted to those in the corresponding one-dimensional (1D) geometry, no matter the potentials inside are rotationally symmetric or not. These results are first numerically observed and then are proved by mathematical methods. For spatially varying Kerr nonlinearity, 2D exact peakons are explicitly obtained, giving birth to families of stable square peakons in the rotationally symmetric potentials and rhombic peakons in the nonrotationally symmetric potentials. By adiabatic excitation, different types of 2D peakons can be transformed stably and reciprocally. Under periodic and mixed perturbations, the 2D stable peakons can also travel stably along the spatially moving potential well, which implies that it is feasible to manage the propagation of the light by regulating judiciously the potential well. However, the vast majority of high-order vortex peakons are vulnerable to instability, which is demonstrated by the linear-stability analysis and by direct numerical simulations of propagation of peakon waveforms. In addition, 3D exact and numerical peakon solutions including the rotationally symmetric and the nonrotationally symmetric ones are obtained, and we find that incompletely rotationally symmetric peakons can occur stably in completely rotationally symmetric DSE potentials. The 3D fundamental peakons can propagate stably in a certain range of potential parameters, but their stability may get worse with the loss of rotational symmetry. Exceptional points and exact peakons in  $n$  dimensions are also summarized.

DOI: [10.1103/PhysRevE.108.064203](https://doi.org/10.1103/PhysRevE.108.064203)

## I. INTRODUCTION

Recently, many intriguing features associated with  $\mathcal{PT}$  symmetry [1], e.g.,  $\mathcal{PT}$ -symmetry-breaking behaviors and stable  $\mathcal{PT}$  nonlinear localized modes have been investigated theoretically and discovered experimentally [2–19]. Meanwhile, the associated exceptional points (EPs), emerging as the fairly unique phase-transition points between the unbroken and the broken phases of  $\mathcal{PT}$  symmetry, are of great significance in the non-Hermitian Hamiltonian and also have crucial applications in other fields such as photonics and electromagnetics [20–24]. The  $\mathcal{PT}$ -symmetric structures can be accomplished in optics by bringing appropriately the gain and loss regions in the waveguide geometry [2,25]. To be more specific, the complex-valued refractive index distribution may totally act as the common  $\mathcal{PT}$ -symmetric optical potentials. Particularly, in the periodic optical lattice potentials, a large number of newfangled characteristics with regard to  $\mathcal{PT}$  symmetry have also been observed successively, such as the double refraction, power oscillation, phase singularity, and secondary emission [26–28].

Over the last dozen years, considerable effort has been devoted to explore the one- and high-dimensional solitons together with their stabilities in non-Hermitian systems with a

variety of optical potentials, ranging from the Scarf-II potential [2,6,29], Gaussian potential [5,30,31], harmonic potential [32,33], Rosen-Morse potential [34], double- $\delta$  potential [35,36], super-Gaussian potential [37], optical lattices or superlattices [4,7,38–42], time-dependent harmonic-Gaussian potential [43], photonic systems [44], to many other relevant physical systems [45–52]. Besides, the special optical peakons, flat-top solitons, and double-hump solitons can reside stably in the one-dimensional (1D)  $\mathcal{PT}$ -symmetric potentials related to the Dirac  $\delta(x)$  function [53]. However, what happens in the higher-dimensional cases? This issue on account of the complicated calculations involved has barely been discussed yet including the EPs and peakon solutions induced by the higher-dimensional and non-Hermitian  $\mathcal{PT}$  symmetry.

In this paper, we aim to investigate the key features of EPs and the propagation dynamics of different types of peakons in the higher-dimensional (e.g., 2D, 3D) inhomogeneous nonlinear Schrödinger (NLS) equation with the spatially varying nonlinearity and non-Hermitian  $\mathcal{PT}$ -symmetric DSE potential [2,3]

$$i\partial_z\psi = -\nabla_{\mathbf{r}}^2\psi + [V(\mathbf{r}) + iW(\mathbf{r})]\psi - g(\mathbf{r})|\psi|^2\psi, \quad (1)$$

where  $\psi \equiv \psi(\mathbf{r}, z)$  denotes the complex-valued wave function related to the dimensionless slowly varying light field amplitude,  $\mathbf{r} = (x_1, x_2, \dots, x_n)$  stands for the  $n$ -dimensional

\*Corresponding author: [zyyan@mrc.iss.ac.cn](mailto:zyyan@mrc.iss.ac.cn)

space or time coordinate,  $z$  describes the propagation distance of light beam,  $\nabla_{\mathbf{r}}^2 = \sum_{k=1}^n \partial^2 / (\partial x_k^2)$  is the  $n$ -dimensional Laplace operator, and  $g(\mathbf{r})$  characterizes the spatially varying cubic-nonlinear strength. The complex potential  $V(\mathbf{r}) + iW(\mathbf{r})$  is regarded as  $\mathcal{PT}$  symmetric provided that  $V(\mathbf{r}) = V(-\mathbf{r})$  and  $W(-\mathbf{r}) = -W(\mathbf{r})$ . In optics, the real part  $V(\mathbf{r})$  has to do with the refractive-index distribution of the optical waveguide whereas the imaginary part  $W(\mathbf{r})$  plays an important role in the gain or loss of light beam. Besides, Eq. (1) can also be represented as an alternative variational form  $i\partial\psi/\partial z = \delta\mathcal{H}(\psi)/\delta\psi^*$  with  $\mathcal{H}(\psi) = \int_{\mathbb{R}^n} \{ |\nabla_{\mathbf{r}}\psi|^2 + [V(\mathbf{r}) + iW(\mathbf{r})]|\psi|^2 - \frac{g(\mathbf{r})}{2}|\psi|^4 \} d\mathbf{r}$ , with the asterisk symbolizing the complex conjugate. Finally, according to the definition of total optical power:  $P(z) = \int_{\mathbb{R}^n} |\psi(\mathbf{r}, z)|^2 d\mathbf{r}$ , one can obtain that the rate of total power change with respect to the propagation distance is  $dP(z)/dz = 2 \int_{\mathbb{R}^n} W(\mathbf{r})|\psi(\mathbf{r}, z)|^2 d\mathbf{r}$ . In actual applications, the intensity  $|\psi(\mathbf{r}, z)|^2$  is a localized even function of  $\mathbf{r}$ , and simultaneously the  $\mathcal{PT}$  symmetry requires  $W(\mathbf{r})$  to be an odd function of  $\mathbf{r}$ , thus we have  $dP(z)/dz = 0$ , which implies that the total power  $P$  is a conserved quantity.

The main contributions of this paper can be concluded as follows:

(1) We introduce a class of higher-dimensional  $\mathcal{PT}$ -symmetric potentials constituted by delta-sign-exponential (DSE) functions to show that the exceptional points in the non-Hermitian Hamiltonian can be converted to those in the corresponding 1D geometry.

(2) In the spatially varying Kerr nonlinearity, we found the 2D exact peakon solutions of Eq. (1). Families of stable square peakons in the rotationally symmetric potentials and stable rhombic peakons in the nonrotationally symmetric potentials are obtained.

(3) By adiabatic excitation, different types of 2D peakons can be transformed stably and reciprocally. Under periodic and mixed perturbations, the 2D stable peakons can also travel stably along the spatially moving potential well, which implies that it is feasible to manage the propagation of the light by regulating judiciously the potential well. However, the vast majority of high-order vortex peakons are vulnerable to instability, which is illustrated by the linear-stability spectrum and by the nonlinear propagation of peakon waveforms.

(4) We also find the 3D exact and numerical peakon waveforms including the rotationally symmetric and the non-rotationally symmetric ones, and we show that incompletely rotationally symmetric peakons can be stable in completely rotationally symmetric DSE potentials. The 3D fundamental peakons can usually maintain stable in a certain range of potential parameters, but their stability may get worse with the loss of rotational symmetry.

(5) Moreover, exceptional points and exact peakons in  $n$  dimensions are summarized. Our results open new possibilities for designing functional physical devices or optical materials with selectable directional propagation.

The remainder of this paper is arranged as follows. In Sec. II, we first numerically investigate the EPs by establishing the 2D  $\mathcal{PT}$ -symmetric DSE potential, and then try to theoretically prove the findings obtained numerically. In Sec. III, we introduce the related approaches and properties to seek exact and numerical nonlinear localized modes. We employ the analytical theory to represent the 2D exact peakons

explicitly, and numerical techniques to capture 2D high-order peakons and families of 2D fundamental peakons in the internal modes, and further analyze their stability, as well as the propagation dynamics. In Sec. IV, we explore the 3D peakons and stabilities in the rotationally symmetric and the nonrotationally symmetric DSE potentials, respectively, and subsequently summarize the EP formula and explicit expression of exact peakons in  $n$  dimensions. Finally, we conclude the main findings with a discussion in Sec. V.

## II. EPS INDUCED BY THE 2D $\mathcal{PT}$ SYMMETRY

For the case of linear regime, that is,  $g(\mathbf{r}) \equiv 0$  in Eq. (1), we will mainly concentrate on the analysis of EPs in the following spectral problem of the 2D non-Hermitian  $\mathcal{PT}$ -symmetric Hamiltonian:

$$\bar{\mathcal{H}}\Psi(x, y) = \lambda\Psi(x, y), \quad \bar{\mathcal{H}} = -\nabla^2 + V(x, y) + iW(x, y), \quad (2)$$

by introducing a new class of  $\mathcal{PT}$ -symmetric delta-sign-exponential (DSE) function potential

$$\begin{aligned} V(x, y) &= -\alpha\delta(x) - \beta\delta(y), \\ W(x, y) &= W_0[\alpha \operatorname{sgn}(x)e^{-\alpha|x|/2} + \beta \operatorname{sgn}(y)e^{-\beta|y|/2}], \end{aligned} \quad (3)$$

where  $\alpha, \beta > 0$ , and  $W_0$  are all real parameters used to regulate the non-Hermitian potential. Numerically, the Dirac  $\delta(x)$  function is usually approximated by the limit of the following Gaussian function  $\delta(x) = \lim_{\epsilon \rightarrow 0^+} G(x, \epsilon)$ ,  $G(x, \epsilon) = \frac{1}{\epsilon\sqrt{\pi}} e^{-x^2/\epsilon^2}$ . Taking the computational complexity and accuracy into consideration, we always take  $\epsilon = 0.05$  in the numerical calculation below.

Due to the spatial symmetry of DSE potential (3), the EPs always occur in pairs. If certain  $W_0$  is a positive EP, then  $-W_0$  is the associated negative EP, which can be clearly observed from the two symmetric blue curves in Fig. 1(a). For convenience, the notation  $\bar{W}_0$  is used to represent the positive EP. Figure 1(a) shows that the positive EP  $\bar{W}_0$  monotonically increases as  $\alpha = \beta$  rises, which implies that the deeper the rotationally symmetric potential well is, the easier it is to generate the fully real spectrum. For  $\alpha = 1, 2, 3, 4$ , the concrete approximation values for EPs are displayed in Fig. 1(b). More importantly, as  $\alpha \neq \beta$ , Fig. 1(b) also shows that, if  $\alpha \leq \beta$ , the positive EP  $\bar{W}_0$  will grow when  $\alpha$  is increasing (e.g.,  $\alpha = 1, 2$  for  $\beta = 2$ ); else if  $\alpha \geq \beta$ ,  $\bar{W}_0$  will preserve unchanged though  $\alpha$  varies (e.g.,  $\alpha = 2, 3, 4$  for  $\beta = 2$ ). To verify the accuracy of these EPs, we take, for example,  $\alpha = 3, \beta = 2$ , in order to test the specific eigenvalue spectrum at  $W_0 = 1.74$  and  $1.75$ , respectively. As expected, at  $W_0 = 1.74$  the whole spectrum is completely real while it turns out to be complex along with some imaginary parts at  $W_0 = 1.75$  [see Figs. 1(c), 1(d)]. According to the symmetry of the potential (3), it is easily deducible that the situation of the exceptional point at  $\alpha = 2, \beta = 3$  ought to be the same as that at  $\alpha = 3, \beta = 2$  before. In other words, the positive EP at  $\alpha = 2, \beta = 3$  is also  $\bar{W}_0 = 1.75$ . More than that, when  $\alpha = 2$  and only if  $\beta \geq 2$ , the same circumstance occurs. Figure 1(e) illustrates the fact that the spectrum always remains entirely real at  $W_0 = 1.74$  as  $\beta$  increases but becomes complex valued with some imaginary parts appearing in the spectrum at  $W_0 = 1.75$ . This means that

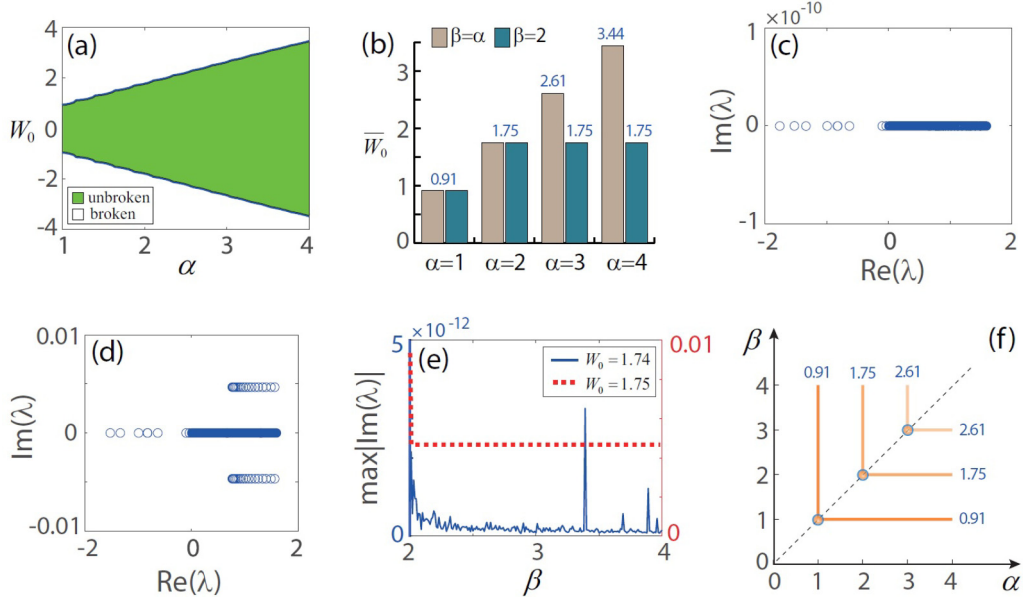


FIG. 1. (a) The  $\mathcal{PT}$ -symmetry-breaking curves (blue) consisting of EPs induced by the 2D non-Hermitian potential (3) with  $\alpha = \beta$ , between which the green area symbolizes the unbroken  $\mathcal{PT}$  symmetry, the remaining white region displays the broken phase. Notice that the 1D bifurcation eigenvalue curves related to eigenvector coalescence have been systematically examined in a previous work, see Ref. [53]. (b) Comparison of several EPs between rotationally symmetric potential (3) with  $\alpha = \beta$  and nonrotationally symmetric potential with  $\alpha \neq \beta$ , where the vertical coordinate  $\bar{W}_0$  stands for the positive EP. (c) All-real spectrum:  $W_0 = 1.74$ , (d) complex spectra:  $W_0 = 1.75$ , of nonrotationally symmetric potential with  $\alpha = 3$ ,  $\beta = 2$ . (e) The maximum absolute value of the imaginary parts of the eigenvalues  $\lambda$  evolves with  $\beta$  when  $W_0 = 1.74$  and  $W_0 = 1.75$ , where  $\alpha = 2$ . (f) Regular arrangement of EPs in the  $(\alpha, \beta)$  space.

$\bar{W}_0 = 1.75$  for any  $\beta \geq 2$ , if  $\alpha = 2$ . A natural problem arises, namely, for fixed value of  $\alpha$  (or  $\beta$ ), is the exceptional point always the same for any  $\beta \geq \alpha$  (or  $\alpha \geq \beta$ )? The answer is yes, and it comes from numerical experiments.

Combining the conclusions of Figs. 1(b) and 1(e), and through plenty of numerical calculations, a nice result is shown in Fig. 1(f), namely that for any  $(\alpha, \beta) \in \mathbb{R}_+^2$ , the positive EP always holds the same as that at  $(\varrho, \varrho)$  with  $\varrho = \min(\alpha, \beta)$ , namely  $\bar{W}_0(\alpha, \beta) \equiv \bar{W}_0(\varrho, \varrho)$  ( $\forall \alpha > 0, \beta > 0$ ). It implies that the EPs in nonrotationally symmetric potential (3) with  $\alpha \neq \beta$  can all boil down to those in rotationally symmetric potential (3) with  $(\varrho, \varrho)$ .

*Proposition 1.* For  $\forall (\alpha, \beta) \in \mathbb{R}_+^2$ , one has  $\bar{W}_0(\alpha, \beta) = \bar{W}_0(\varrho, \varrho) = \bar{W}_0(\varrho)$ , where  $\varrho = \min(\alpha, \beta)$  signifies the minimum of  $\alpha$  and  $\beta$ .

*Proof.* We might as well suppose that  $\beta \geq \alpha > 0$ . Let

$$\tilde{\mathcal{H}}_\alpha = -\partial_x^2 - \alpha\delta(x) + iW_0\alpha\text{sgn}(x)e^{-\alpha|x|/2}, \quad (4)$$

$$\tilde{\mathcal{H}}_\beta = -\partial_y^2 - \beta\delta(y) + iW_0\beta\text{sgn}(y)e^{-\beta|y|/2}. \quad (5)$$

Exerting the variable substitution  $y = \alpha x/\beta$  on  $\tilde{\mathcal{H}}_\beta$  yields that

$$\tilde{\mathcal{H}}_\beta = \frac{\beta^2}{\alpha^2} \left[ -\partial_x^2 - \alpha\delta(x) + i \left( \frac{\alpha}{\beta} W_0 \right) \alpha \text{sgn}(x) e^{-\alpha|x|/2} \right]. \quad (6)$$

Comparing the eigenvalues of two Hamiltonian operators (6) and (4), we can arrive at the corresponding relationship

between their EPs as follows:

$$\bar{W}_{0\alpha} = \frac{\alpha}{\beta} \bar{W}_{0\beta} \Leftrightarrow \bar{W}_{0\beta} = \frac{\beta}{\alpha} \bar{W}_{0\alpha}, \quad (7)$$

where  $\bar{W}_{0\alpha}$  and  $\bar{W}_{0\beta}$  represent the positive EPs of the Hamiltonian operators (4) and (5), respectively, namely  $\bar{W}_{0\alpha} \equiv \bar{W}_0(\alpha)$  and  $\bar{W}_{0\beta} \equiv \bar{W}_0(\beta)$ . Equation (7) unveils that the range of parameter for the Hamiltonian operator (4) having the all-real spectrum is  $W_0 \in (-\bar{W}_{0\alpha}, \bar{W}_{0\alpha})$  if and only if the range of parameter for the Hamiltonian operator (5) having the all-real spectrum is  $W_0 \in (-\frac{\beta}{\alpha}\bar{W}_{0\alpha}, \frac{\beta}{\alpha}\bar{W}_{0\alpha}) \supseteq (-\bar{W}_{0\alpha}, \bar{W}_{0\alpha})$ .

On the other hand, we assume that the eigenvalues and eigenstates of  $\tilde{\mathcal{H}}_\alpha$  and  $\tilde{\mathcal{H}}_\beta$  are

$$\tilde{\mathcal{H}}_\alpha : \{\mu_j\}_{j=0}^\infty, \{|\phi_j(x)\rangle\}_{j=0}^\infty \in L^2(\mathbb{R}), \quad (8)$$

$$\tilde{\mathcal{H}}_\beta : \{\nu_k\}_{k=0}^\infty, \{|\psi_k(x)\rangle\}_{k=0}^\infty \in L^2(\mathbb{R}), \quad (9)$$

then  $\tilde{\mathcal{H}}|\phi_j(x)\psi_k(x)\rangle = (\tilde{\mathcal{H}}_\alpha + \tilde{\mathcal{H}}_\beta)|\phi_j(x)\rangle|\psi_k(x)\rangle = (\mu_j + \nu_k)|\phi_j(x)\psi_k(x)\rangle$ . It means that the eigenvalues and eigenstates of the 2D linear Hamiltonian (2) with the potential (3) are  $\tilde{\mathcal{H}} : \{\mu_j + \nu_k\}_{j,k=0}^\infty, \{|\phi_j(x)\psi_k(x)\rangle\}_{j,k=0}^\infty \in L^2(\mathbb{R})$ . Thus,  $\tilde{\mathcal{H}} = \tilde{\mathcal{H}}_\alpha + \tilde{\mathcal{H}}_\beta$  possesses a completely real spectrum  $\Leftrightarrow \tilde{\mathcal{H}}_\alpha$  and  $\tilde{\mathcal{H}}_\beta$  simultaneously admit entirely real spectrum  $\Leftrightarrow W_0 \in (-\bar{W}_{0\alpha}, \bar{W}_{0\alpha})$ . Due to the assumption  $\beta \geq \alpha$  and  $\varrho = \min(\alpha, \beta)$ , we have  $\bar{W}_0(\alpha, \beta) = \bar{W}_{0\alpha} = \bar{W}_0(\varrho)$ . Then taking  $\alpha = \beta = \varrho$ , one again yields  $\bar{W}_0(\varrho, \varrho) = \bar{W}_0(\varrho)$ . Therefore, we complete this proof.

We point out that the proposition can help us to find the EPs in the higher-dimensional parameter spaces, where usually a huge amount of computation is necessary.

### III. 2D PEAKON SOLUTIONS IN THE $\mathcal{PT}$ -SYMMETRIC DSE POTENTIAL AND STABILITY

In this section, first we will set about seeking the explicit representation of the 2D exact peakons in the nonlinear wave system (1) with the  $\mathcal{PT}$ -symmetric DSE potential (3), then numerically explore families of fundamental peakons including rotationally symmetric and nonrotationally symmetric around them as well as high-order numerical peakons. Some significant properties such as the dynamical stability related to these peakons are also investigated in detail.

#### A. Theoretical analysis of stationary nonlinear modes and stability

We mainly devote ourselves to the nonlinear modes in the steady-state form  $\psi(\mathbf{r}, z) = \phi(\mathbf{r})e^{i\mu z}$  with  $\mu$  being a real propagation constant and  $\phi(\mathbf{r})$  a localized nonlinear mode satisfying  $\phi(\mathbf{r}) \in \mathbb{C}[\mathbf{r}]$  and  $\lim_{|\mathbf{r}| \rightarrow \infty} \phi(\mathbf{r}) = 0$  such that Eq. (1) yields the following complex-valued and variable-coefficient second-order partial differential equation obeyed by the nonlinear localized modes  $\phi(\mathbf{r})$

$$(\nabla_{\mathbf{r}}^2 - \mu)\phi = [V(\mathbf{r}) + iW(\mathbf{r}) - g(\mathbf{r})|\phi|^2]\phi, \quad (10)$$

which can actually be regarded as a generalized Poisson equation with a self-induced inhomogeneous term.

Since the complex-valued nonlinear mode  $\phi(\mathbf{r})$  can be expressed as the exponential form  $\phi(\mathbf{r}) = A(\mathbf{r})\exp[i\theta(\mathbf{r})]$ , with  $A(\mathbf{r})$  being a real amplitude function yet  $\theta(\mathbf{r})$  a real phase function, one can readily derive the coupled nonlinear wave equations with respect to  $A(\mathbf{r})$  and  $\theta(\mathbf{r})$  as follows:

$$\begin{aligned} \nabla_{\mathbf{r}} \cdot [A^2(\mathbf{r})\nabla_{\mathbf{r}}\theta(\mathbf{r})] &= A^2(\mathbf{r})W(\mathbf{r}), \\ \Delta_{\mathbf{r}}A(\mathbf{r}) &= [V(\mathbf{r}) - g(\mathbf{r})A^2(\mathbf{r}) \\ &\quad + |\nabla_{\mathbf{r}}\theta(\mathbf{r})|^2 + \mu]A(\mathbf{r}). \end{aligned} \quad (11)$$

We can seek the soliton solutions of Eq. (10) by using both analytical approaches (see Appendix A) and numerical methods (see Appendix B). Besides, alternative numerical algorithms can also be utilized to solve Eq. (10) for 1D and high-dimensional nonlinear localized modes under the zero-boundary condition [54–56]. In this paper, we mainly take advantage of the modified squared-operator iteration method in search for the high-order numerical nonlinear modes, since it can reach a higher precision and is of great convenience in higher dimensions. Nonetheless, we have to point out that, in several certain types of  $\mathcal{PT}$  potential wells, exact solitons tend to play a crucial role in searching for families of stable numerical nonlinear modes (see Refs. [8,43]).

Once the nonlinear localized modes of Eq. (1) are attained in the steady-state form  $\psi(\mathbf{r}, z) = \phi(\mathbf{r})e^{i\mu z}$ , no matter exact or numerical, we can further analyze their linear stability by the following small perturbation:

$$\tilde{\psi}(\mathbf{r}, z) = \psi(\mathbf{r}, z) + \delta[u_1(\mathbf{r})e^{i\nu z} + u_2^*(\mathbf{r})e^{-i\nu^*z}]e^{i\mu z}, \quad (12)$$

where  $|\delta| \ll 1$  is an infinitesimal parameter, both  $u_1(\mathbf{r})$  and  $u_2(\mathbf{r})$  are the eigenfunctions under perturbation, and  $\nu$  measures the rate of expansion of the perturbation instability. The perturbed solution is substituted into Eq. (1) to the linear-stability eigenvalue problem (considering the linear terms

of  $\delta$ )

$$\begin{bmatrix} \tilde{L}_1 & \tilde{L}_2 \\ -\tilde{L}_2^* & -\tilde{L}_1^* \end{bmatrix} \begin{bmatrix} u_1(\mathbf{r}) \\ u_2(\mathbf{r}) \end{bmatrix} = \nu \begin{bmatrix} u_1(\mathbf{r}) \\ u_2(\mathbf{r}) \end{bmatrix}, \quad (13)$$

where  $\tilde{L}_1 = \nabla_{\mathbf{r}}^2 - [V(\mathbf{r}) + iW(\mathbf{r}) + 2g(\mathbf{r})|\phi(\mathbf{r})|^2 - \mu]$ ,  $\tilde{L}_2 = g(\mathbf{r})\phi^2(\mathbf{r})$ .

It is evident that the steady-state nonlinear modes are identified as linearly unstable only if  $\nu$  has a negative imaginary part, otherwise the nonlinear modes are linearly stable. The whole linear-stability spectrum can be approximately calculated by the Fourier collocation method (see Ref. [57]). Although the linear stability can conveniently predict the parameter range of stable nonlinear modes, it is just one necessary yet not sufficient condition of true stability. Thus it is imperative that the propagation simulation technique of nonlinear waves need to be implemented to further validate the stability of nonlinear modes.

#### B. Explicit representation of 2D peakons and stability

Here the formation of the bright spatial peakons and their stability will be explored in the 2D geometries determined by the  $\mathcal{PT}$ -symmetric DSE potential (3) and spatially varying Kerr nonlinearity. Under this circumstance, Eq. (1) becomes

$$\begin{aligned} i\frac{\partial\psi}{\partial z} + \left(\frac{\partial^2}{\partial x^2} + \frac{\partial^2}{\partial y^2}\right)\psi \\ + [V(x, y) + iW(x, y)]\psi + g(x, y)|\psi|^2\psi \\ = 0. \end{aligned} \quad (14)$$

If we take the spatially varying strength of Kerr nonlinearity as  $g(x, y) = e^{\alpha|x|} + e^{\beta|y|}$ , then the exact peakon solution of Eq. (14) can be deduced in the following form:

$$\psi(x, y, z) = \phi(x, y)e^{i\varphi(x, y)}e^{i(\alpha^2 + \beta^2)z/4}, \quad (15)$$

where the amplitude function  $\phi(x, y)$  and phase  $\varphi(x, y)$  are

$$\begin{aligned} \phi(x, y) &= \frac{2W_0}{3} \exp\left(-\frac{\alpha|x| + \beta|y|}{2}\right), \\ \varphi(x, y) &= -\frac{2W_0}{3} \int_{(0,0)}^{(x,y)} e^{-\alpha|x|/2} dx + e^{-\beta|y|/2} dy. \end{aligned} \quad (16)$$

Next we are going to discuss peakons and their stability in two cases:  $\alpha = \beta$  (square peakons) and  $\alpha \neq \beta$  (rhombic peakons).

Notice that we choose the spatially dependent Kerr nonlinearity as  $g(x, y) = e^{\alpha|x|} + e^{\beta|y|}$ . It is a function that grows exponentially, but it may be truncated in a very limited domain of space in an experimental physical setting. In fact, one can also choose other bounded functions or constant functions of  $x, y$ , e.g.,  $g(x, y) = e^{-(\gamma_1 x^2 + \gamma_2 y^2)}$  ( $\gamma_{1,2} > 0$ ) or  $g(x, y) = 1$ . Even if these special cases may not make Eq. (14) to possess exact peakon solutions, from Eq. (14) we can also get similar results, that is, 2D numerically found peakons. We also point out that without the assumption of the exponentially growing of the spatially varying strength of Kerr nonlinearity, we have obtained in a recent work [58], 1D peakons and double-hump solitons in the  $\mathcal{PT}$ -symmetric Dirac- $\delta(x)$ -Scarff-II optical potentials.

*Square peakons.* When taking  $\alpha = \beta = 2$  and  $W_0 = 0.2$ , which corresponds to the case of linear  $\mathcal{PT}$  unbroken phase

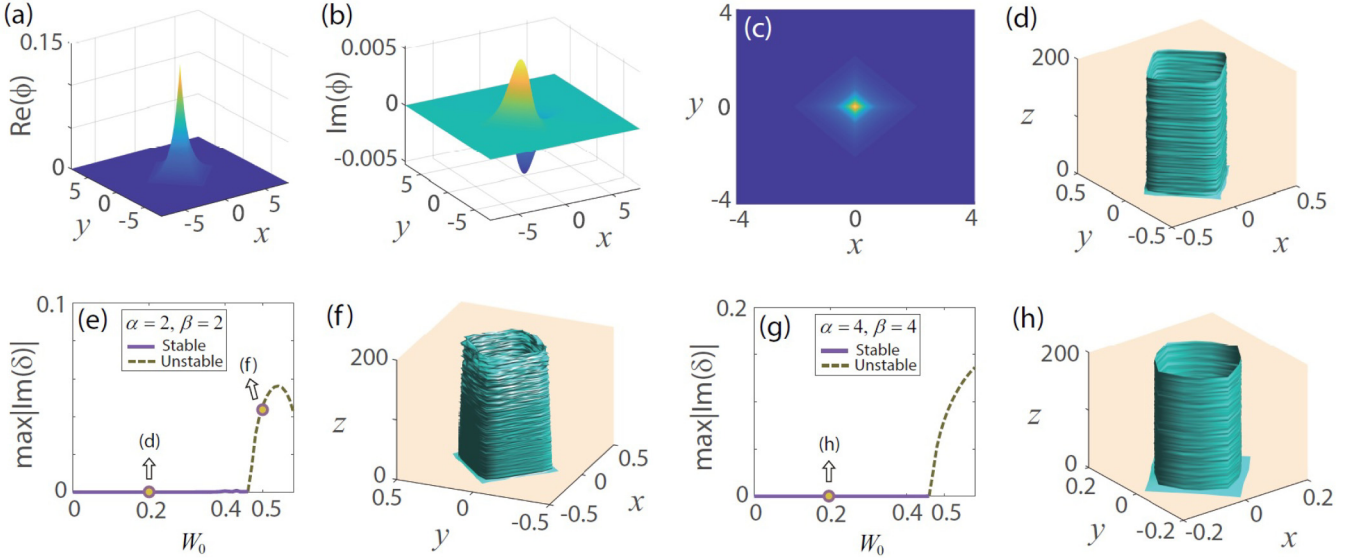


FIG. 2. (a) Real part, (b) imaginary part, and (c) intensity of the 2D exact rotationally symmetric fundamental peakon (16) with  $\alpha = \beta = 2$ ,  $W_0 = 0.2$ . Linear stability curves of the 2D peakon (16) with (e)  $\alpha = \beta = 2$ , (g)  $\alpha = \beta = 4$ . (d) Stable propagation:  $\alpha = \beta = 2$ ,  $W_0 = 0.2$ , which corresponds to the case of linear  $\mathcal{PT}$  unbroken phase [cf. Fig. 1(a)]; (f) unstable propagation:  $\alpha = \beta = 2$ ,  $W_0 = 0.5$ , which corresponds to the case of linear  $\mathcal{PT}$  unbroken phase [cf. Fig. 1(a)]; (h) stable propagation:  $\alpha = \beta = 4$ ,  $W_0 = 0.2$ , which corresponds to the case of linear  $\mathcal{PT}$  unbroken phase [cf. Fig. 1(a)].

[cf. Fig. 1(a)], the profile of the stationary peakon solution (16) has been exhibited with its real part, imaginary part, and intensity in Figs. 2(a)–2(c). From the perspective of the intensity, we can clearly observe that the cross section of the peakon is square, thus we also call it square peakon, which is rotationally symmetric in  $x$  and  $y$  coordinate directions. By performing propagation simulation of nonlinear waves, we find that the square peakon can remain stable in long-distance propagation; this stable evolution is shown in Fig. 2(d) by contour lines with half the maximum of its intensity. In fact, the linear stability plot in Fig. 2(e) reveals that the square peakon (16) can travel stably in a wide range of  $W_0$  as  $\alpha = \beta = 2$ . But beyond a certain parameter range of the parameter  $W_0$ , such as for  $W_0 = 0.5$ , the square peakon will become relatively unstable [see Fig. 2(f)]. Moreover, even if increasing simultaneously the values of  $\alpha$  and  $\beta$ , we can also attain a stable set of peakons by the linear stability analysis [see Figs. 2(g), 2(h)]. It fully shows that the peakon (16) is relatively robust to the change of refractive index distribution, but is not robust to the change of the gain-loss distribution.

**Rhombic peakons.** Fixing  $\beta = 2$ , we successively take, for example,  $\alpha = 1$  and  $\alpha = 3$ , in order to analyze the linear stability of peakons, leading to Figs. 3(a1), 3(b1), which exhibit that the linearly stable range of peakons expands as  $\alpha$  increases. Especially at  $W_0 = 0.2$ , two distinguished forms of rhombus peakons can be generated [see Figs. 3(a2), 3(b2)]; more importantly, both of them can also propagate stably over a long distance, as displayed in Figs. 3(a3), 3(b3). From Figs. 3(a2), 3(b2) or Figs. 3(a3), 3(b3), we observe that in the direction in which the potential well is stronger, the rhombic peakon is slimmer. For instance, if  $\alpha > \beta$ , which means the strength in the  $x$  direction is higher than that in the  $y$  direction for the real part of the DSE potential (3), then the width of the rhombic peakon in the  $x$  direction will be narrower than that in the  $y$  direction.

### C. Dynamical excitations of 2D exact peakons

Here we aim to give birth to additional stable peakons from the known input determined by Eq. (15), just by making the potential well parameters adiabatically depending on the propagation distance, i.e.,  $\alpha \rightarrow \alpha(z)$ ,  $\beta \rightarrow \beta(z)$  or  $W_0 \rightarrow W_0(z)$  (cf. Ref. [43]). It means that three adiabatic switches are necessary to be simultaneously exerted on the DSE potential (3). At this time, Eq. (1) turns into

$$i \frac{\partial \psi}{\partial z} + \left[ \frac{\partial^2}{\partial x^2} + \frac{\partial^2}{\partial y^2} - U(x, y, z) + g(x, y) |\psi|^2 \right] \psi = 0, \quad (19)$$

where  $U(x, y, z) \equiv V(x, y, z) + iW(x, y, z)$  denotes the complex  $z$ -dependent potential,  $V \equiv V(x, y, z)$  and  $W \equiv W(x, y, z)$  are given by Eq. (3) with  $\alpha \rightarrow \alpha(z)$ ,  $\beta \rightarrow \beta(z)$  and  $W_0 \rightarrow W_0(z)$ , i.e.,

$$\begin{aligned} V(x, y, z) &= -\alpha(z)\delta(x) - \beta(z)\delta(y), \\ W(x, y, z) &= W_0(z)[\alpha(z)\text{sgn}(x)e^{-\alpha(z)|x|/2} \\ &\quad + \beta(z)\text{sgn}(y)e^{-\beta(z)|y|/2}]. \end{aligned} \quad (18)$$

Alternatively, the adiabatic variation of potential parameters  $\alpha(z)$ ,  $\beta(z)$ , and  $W_0(z)$  can be both selected as the following path form:

$$\chi(z) = \begin{cases} (\chi_2 - \chi_1) \sin\left(\frac{\pi z}{z_{\max}}\right) + \chi_1, & 0 \leq z < \frac{z_{\max}}{2}, \\ \chi_2, & z \geq \frac{z_{\max}}{2}, \end{cases} \quad (19)$$

where  $\chi_1$  and  $\chi_2$  characterize the initial and final values in the process of excitation, respectively.

For illustration, we only exert the single-parameter adiabatic variation  $\alpha \rightarrow \alpha(z)$  on the DSE potential (3), i.e., always keeping  $\beta(z) \equiv \beta$  and  $W_0(z) \equiv W_0$  constants in the potential (18). The 2D exact peakon (15) is taken as an initial condition

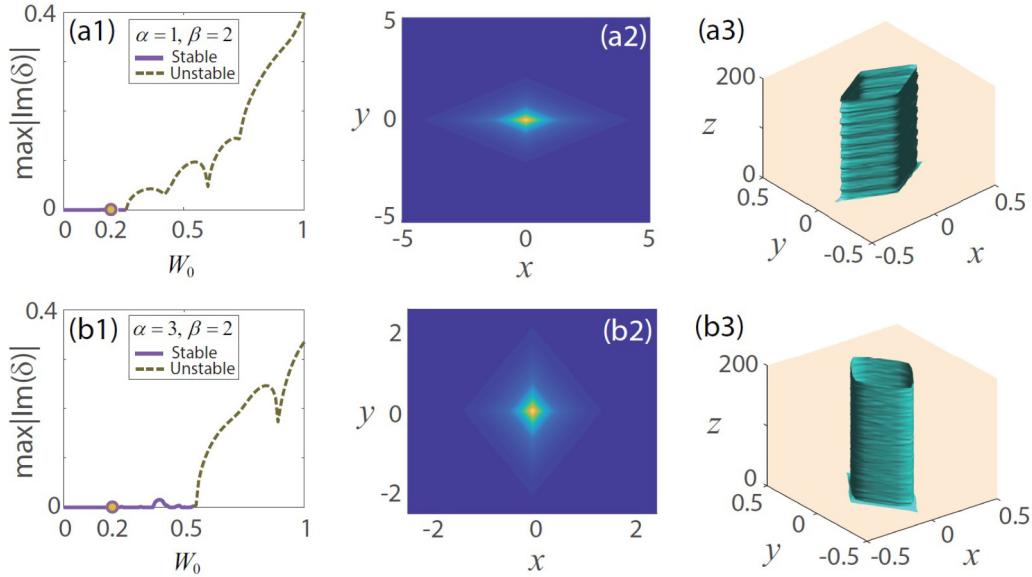


FIG. 3. (a) Linear stability curves of the 2D nonrotationally symmetric peakon (16) with (a1)  $\alpha = 1, \beta = 2$ , (a2)  $\alpha = 3, \beta = 2$ . The corresponding soliton and its stable propagation: (a2), (a3)  $\alpha = 1, \beta = 2, W_0 = 0.2$ , (b2), (b3)  $\alpha = 3, \beta = 2, W_0 = 0.2$ .

with  $\psi(x, y, 0)$ , and its evolution is governed by Eq. (17). As is well known, it is more than easy to excite stably from a rotationally symmetric soliton to another rotationally symmetric soliton, or from a nonrotationally symmetric soliton to another nonrotationally symmetric soliton. But whether can a rotationally symmetric soliton be stably transformed to a nonrotationally symmetric soliton, or a nonrotationally symmetric soliton to a rotationally symmetric soliton? It is possible, even for the unsmooth peakons. We can replace  $\alpha(z)$  with  $\chi(z)$  given by Eq. (19), and take  $\beta = 2, W_0 = 0.2, \alpha_1 = 2$ , and  $\alpha_2 = 3$  as an example to generate a stable nonrotationally symmetric rhombic peakon from the initially

rotationally symmetric square peakon given by Eq. (15), as shown in Figs. 4(a1), 4(b1), 4(c1), 4(d1). See also Figs. 4(a2), 4(b2), 4(c2), 4(d2) for the transformation of the nonrotationally symmetric rhombic peakon to a rotationally symmetric square peakon. Therefore, different kinds of 2D peakons can be stably transformed to each other.

**D. Propagation patterns of 2D exact peakons under perturbation**

When the central point of the 2D DSE potential (3) moves with the propagation distance, a question arises whether the

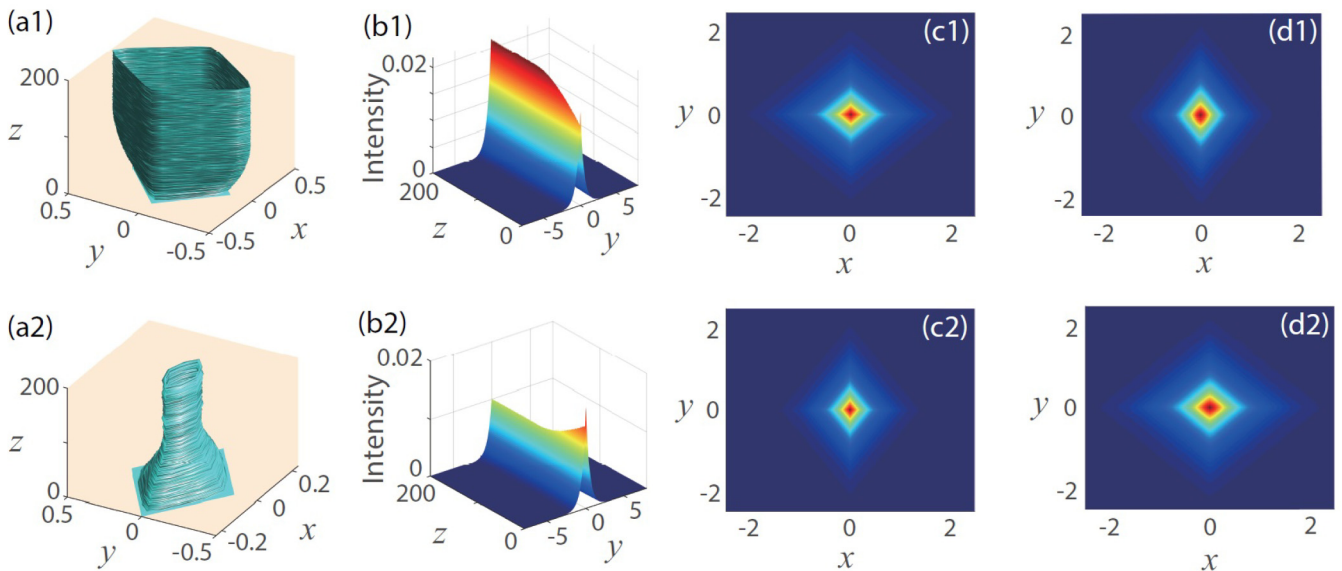


FIG. 4. Transformation of the 2D peakons (16) in Eq. (17) with the potential well (18). The contour evolution of intensity of peakons, the corresponding propagation in  $x = 0$  plane, the initial-state peakon, the final-state peakon: (a1), (b1), (c1), (d1)  $\alpha_1 = 2, \alpha_2 = 3$ ; (a2), (b2), (c2), (d2)  $\alpha_1 = 3, \alpha_2 = 2$ . Here  $\alpha(z)$  is determined by Eq. (19) and other parameters are  $\beta = 2, W_0 = 0.2$ .

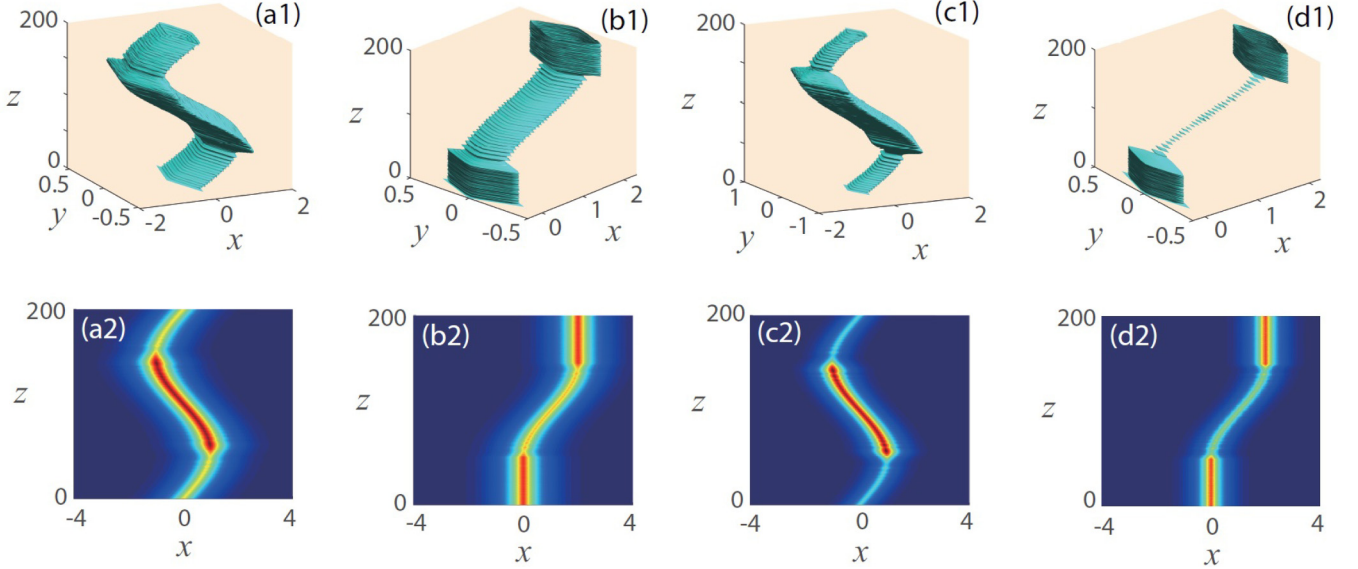


FIG. 5. Propagation patterns of 2D peakons in the perturbed potential well (20). The square peakon at  $(\alpha, \beta) = (2, 2)$ : (a1), (a2) periodic perturbation with  $\tilde{x}_0(z) = \sin(2\pi z/z_{\max})$ ; (b1), (b2) mixed perturbation given by Eq. (21). The rhombic peakon at  $(\alpha, \beta) = (3, 2)$ : (c1), (c2) periodic perturbation with  $\tilde{x}_0(z) = \sin(2\pi z/z_{\max})$ ; (d1), (d2) mixed perturbation given by Eq. (21). The first row is exhibited by the evolution of intensity contour line of 2D peakons and correspondingly the second row displays the propagation of 2D peakons in the  $y = 0$  plane. Here  $W_0 = 0.2$ .

exact peakon (16) can still travel steadily in the nonlinear system (17). To this end, the spatially fixed DSE potential (3) is modified as the following  $z$ -dependent form:

$$\begin{aligned} V(x, y, z) &= -\alpha\delta[x - \tilde{x}_0(z)] - \beta\delta[y - \tilde{y}_0(z)], \\ W(x, y, z) &= W_0\{\alpha\text{sgn}[x - \tilde{x}_0(z)]e^{-\alpha|x - \tilde{x}_0(z)|/2} \\ &\quad + \beta\text{sgn}[y - \tilde{y}_0(z)]e^{-\beta|y - \tilde{y}_0(z)|/2}\}, \end{aligned} \quad (20)$$

where  $\tilde{x}_0(0) = 0$  and  $\tilde{y}_0(0) = 0$  are required so that the exact peakon (15) initially solves Eq. (17) under the DSE potential (20) as  $z = 0$ .

As a matter of convenience, we always take  $\tilde{y}_0(z) = 0$  and mainly consider  $\tilde{x}_0(z)$  in the following two forms:

(1) Periodic perturbation: When the center point of the 2D DSE potential (20) oscillates periodically with the propagation distance along the  $x$ -axis direction, i.e.,  $\tilde{x}_0(z) = \sin(2\pi z/z_{\max})$ , the beam produced by the peakon (16) can still maintain stable propagation like a snake, as is displayed in Figs. 5(a1), 5(a2) for the rotationally symmetric square peakon and Figs. 5(c1), 5(c2) for the nonrotationally symmetric rhombic peakon. Indeed, it can be verified that the center position and wave shape of the final-state 2D peakon is the same as that of the initial state.

(2) Mixed perturbation: When the disturbance path  $\tilde{x}_0(z)$  is selected as the following piecewise function:

$$\tilde{x}_0(z) = \begin{cases} 0, & 0 \leq z \leq \frac{z_{\max}}{4}, \\ \sin\left(\frac{2\pi z}{z_{\max}} - \pi\right) + 1, & \frac{z_{\max}}{4} < z \leq \frac{3z_{\max}}{4}, \\ 2, & \frac{3z_{\max}}{4} < z \leq z_{\max}, \end{cases} \quad (21)$$

the light beam will also travel stably along the moving potential well constrained by Eq. (20), regardless of the existence of inflection points [see Figs. 5(b1), 5(b2) for the square peakon and Figs. 5(d1), 5(d2) for the rhombic peakon].

One can attempt to test some other perturbation paths and find that the 2D stable peakons (16) will also propagate stably along the curve composed of the center position of moving potential well (20). It fully manifests that these peakons are fairly robust no matter the rotationally symmetric square peakons or the nonrotationally symmetric rhombic peakons, and it is also feasible in the 2D geometry to manage the propagation of the light by regulating judiciously the potential well.

### E. 2D numerical peakons in internal modes and high orders

When the external parameters  $\alpha$ ,  $\beta$ , and  $W_0$  of the 2D nonlinear wave system (14) with the DSE potential (3) are given, according to Eqs. (15) and (16), we in fact obtain only one exact peakon corresponding to  $\mu = \frac{1}{4}(\alpha^2 + \beta^2)$ . However, as the internal parameter  $\mu$  varies, are there any other peakons for the 2D system, such as the 2D fundamental peakons and high-order vortex peakons? If so, how do we find them and determine their stability?

First of all, we still choose the external potential parameters  $(\alpha, \beta, w_0) = (2, 2, 0.2)$  as the base point to elaborate how to realize this goal. By virtue of the numerical iteration approach in Appendix B and taking the exact 2D peakon (15) at  $\mu = 2$  as the initial condition, a family of newfangled 2D fundamental peakons can be attained nearby the exact-peakon propagation constant  $\mu = 2$ . Figure 6(a1) exhibits a representative square peakon as  $\mu = 1.8$ . More importantly, the purely real linear stability spectrum in Fig. 6(a2) indicates that this square peakon is linearly stable. Besides, the nonlinear wave propagation technique is also leveraged to further validate the true stability of such a square peakon, as is displayed in Fig. 6(a3), which agrees pretty well with the linear stability result in Fig. 6(a2). The same way can be employed to seek for stable nonrotationally symmetric peakons, with a stable

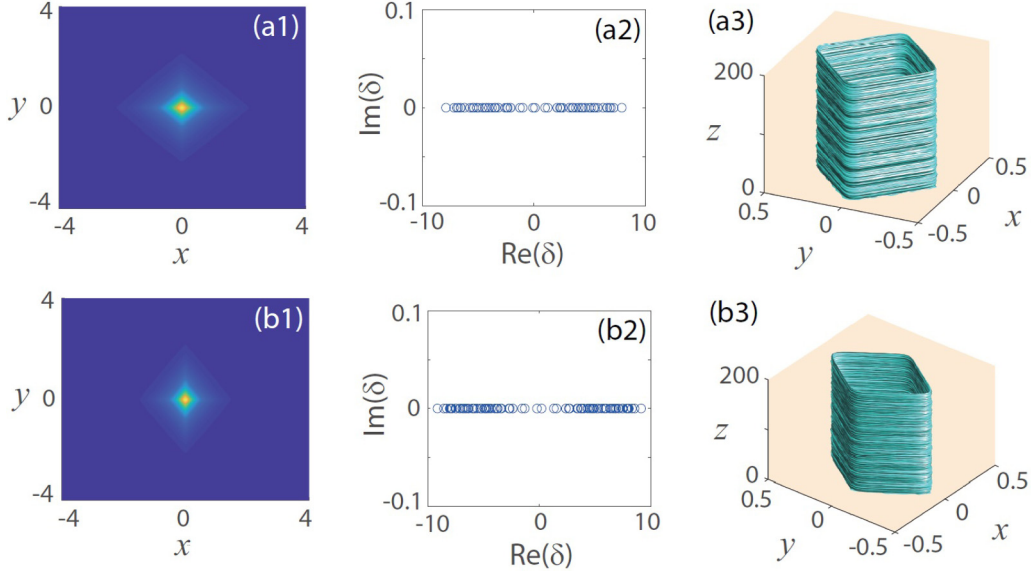


FIG. 6. The square peakon obtained numerically, linear stability spectrum, and stable propagation: (a1, a2, a3)  $\mu = 1.8$ , the other parameters are  $\alpha = 2$ ,  $\beta = 2$ ,  $W_0 = 0.2$ . The rhombic peakon obtained numerically, linear stability spectrum, and stable propagation: (b1), (b2), (b3)  $\mu = 3.2$ , the other parameters are  $\alpha = 3$ ,  $\beta = 2$ ,  $W_0 = 0.2$ .

rhombic peakon generated in Fig. 6(b1), 6(b2), 6(b3). Hence, families of stable rotationally symmetric and nonrotationally symmetric peakons such as the square and the rhombic ones can be produced by regulating properly the internal parameter around the propagation constant corresponding to the stable exact peakons (15).

In sharp contrast to the fundamental peakons, we find that the vast majority of 2D high-order vortex peakons are generally susceptible to losing their stability. For example, by the modified squared-operator iteration method with the following initial condition:

$$\psi(x, y, 0) = A(x^2 + y^2)^{m/2} e^{-(x^2 + y^2)/w^2}, \quad (22)$$

where  $A$  and  $w$  stand for the amplitude and width of initial input wave, respectively, and  $m$  is related to the order of vortex peakons to search for, we can, respectively, capture a five-vortex rotationally symmetric peakon [see Fig. 7(a1)] and a seven-vortex nonrotationally symmetric peakon [see Fig. 7(b1)]. Nonetheless, the linear-stability spectrum with imaginary parts and nonlinear propagation simulation both reveal that they are unstable [see Figs. 7(a2), 7(a3) and 7(b2), 7(b3)].

#### IV. HIGHER-DIMENSIONAL PEAKONS AND THEIR STABILITY

##### A. 3D peakons and their dynamics

As we all know, the 3D spatiotemporal solitons (alias light bullets) have also been a subject of broad significance in nonlinear optics [59–62]. Thus in this section we will focus on elucidating the formation of peakons in the 3D  $\mathcal{PT}$ -symmetric DSE potential. The 3D governing equation with  $\mathcal{PT}$ -symmetric potential and Kerr nonlinearity has the

following normalized form [33]:

$$i \frac{\partial \psi}{\partial z} + \left( \frac{\partial^2}{\partial x^2} + \frac{\partial^2}{\partial y^2} + \frac{\partial^2}{\partial t^2} \right) \psi + U(x, y, t) \psi + g(x, y, t) |\psi|^2 \psi = 0, \quad (23)$$

where  $U(x, y, t) \equiv V(x, y, t) + iW(x, y, t)$ , and the DSE potential in the 3D landscape is

$$V = -\alpha \delta(x) - \beta \delta(y) - \gamma \delta(t), \\ W = W_0 [\alpha \text{sgn}(x) e^{-\alpha|x|/2} + \beta \text{sgn}(y) e^{-\beta|y|/2} + \gamma \text{sgn}(t) e^{-\gamma|t|/2}] \quad (24)$$

with  $\alpha > 0$ ,  $\beta > 0$ ,  $\gamma > 0$ . In the 3D  $\mathcal{PT}$ -symmetric DSE potential (24), if the nonlinear coefficient depending on spatial variation is

$$g(x, y, t) = e^{\alpha|x| + \beta|y|} + e^{\beta|y| + \gamma|t|} + e^{\gamma|t| + \alpha|x|}, \quad (25)$$

then the 3D exact peakon solutions of Eq. (23) can be deduced in the stationary form

$$\psi(x, y, t, z) = \phi(x, y, t) e^{i\varphi(x, y, t)} e^{i(\alpha^2 + \beta^2 + \gamma^2)z/4}, \quad (26)$$

with the amplitude and phase being

$$\phi(x, y, t) = \frac{2W_0}{3} \exp\left(-\frac{\alpha|x| + \beta|y| + \gamma|z|}{2}\right) e^{i\varphi(x, y, t)}, \quad (27)$$

and

$$\varphi(x, y, t) = -\frac{2W_0}{3} \int_{(0,0,0)}^{(x,y,t)} e^{-\frac{1}{2}\alpha|x|} dx + e^{-\frac{1}{2}\beta|y|} dy + e^{-\frac{1}{2}\gamma|t|} dt. \quad (28)$$

First, we still take  $(\alpha, \beta, \gamma) = (2, 2, 2)$  as an example to illuminate the dynamical stability of the 3D analytical peakons (27). Figure 8(a1) exhibits the isosurface profile of



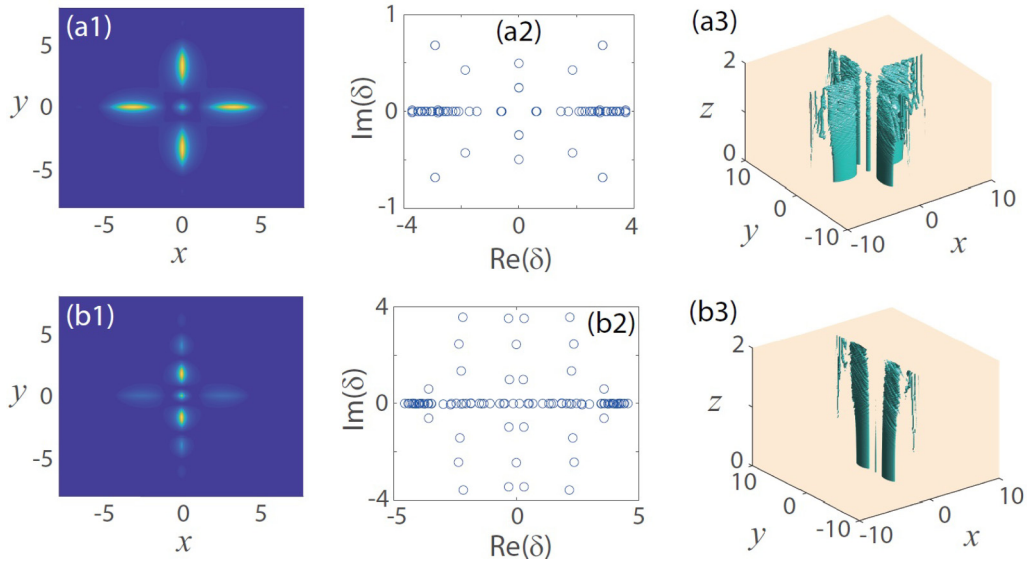


FIG. 7. The high-order rotationally symmetric peakon obtained numerically, linear stability spectrum, and unstable propagation: (a1), (a2), (a3)  $\alpha = 2, \beta = 2, W_0 = 0.2$ . The high-order nonrotationally symmetric peakon obtained numerically, linear stability spectrum, and unstable propagation: (b1), (b2), (b3)  $\alpha = 3, \beta = 2, W_0 = 0.2$ . Here  $\mu = \frac{1}{4}(\alpha^2 + \beta^2)$ .

a prototypical 3D peakon with  $W_0 = 0.2$ , which is completely rotationally symmetric in the  $x$ - $y$ - $t$  three coordinate directions. The nonlinear propagation simulation in Fig. 8(a2) indicates such a 3D peakon is still stable just as in the 2D situation. If increasing the gain-loss strength beyond a certain threshold, such as  $W_0 = 0.5$ , the 3D exact peakon (27) will lose its stability immediately and cannot hold its original wave shape any more in propagation, as shown in Figs. 8(b1), 8(b2).

If sustaining  $W_0 = 0.2$  unchanged and augmenting  $\alpha$  from 2 to other values, such as 3, then the exact peakons will become incompletely rotationally symmetric in the  $x$ - $y$ - $t$  three coordinate directions, but rotationally symmetric in the  $y$ - $t$  two coordinate directions like the corresponding 3D DSE potential (24), as is displayed in Fig. 8(c1). Even so, such 3D peakons can still propagate stably over a relatively long

distance [see Fig. 8(c2)]. Further, simultaneously decreasing  $\gamma$  to another value such as 1, the 3D exact peakon will turn into being utterly nonrotationally symmetric in the  $x$ - $y$ - $t$  three coordinate directions [see Fig. 8(d1)]. At this time, its transmission is relatively susceptible to initial white noise and one can apparently observe periodic oscillation of the wave crest [see Fig. 8(d2)].

Moreover, we also explore numerically the 3D peakons in the internal modes. The incompletely rotationally symmetric peakon in the  $x$ - $y$ - $t$  three coordinate directions can be found and is stable in the completely rotationally symmetric DSE potential (24), shown in Figs. 9(a1), 9(a2). Certainly, by adjusting the internal parameters properly, the peakon can be completely rotationally symmetric and stable too [see Figs. 9(b1), 9(b2)]. In the incompletely rotationally symmet-

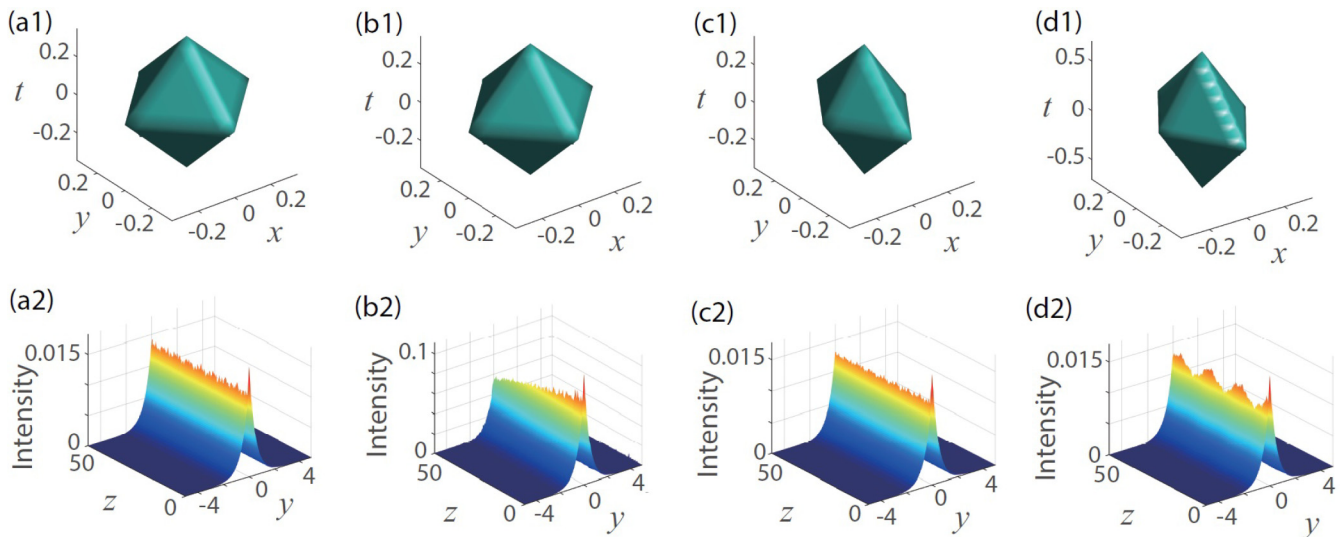


FIG. 8. Isosurface plots and evolution in the  $x = 0$  plane of 3D exact peakons (26) with: (a1), (a2)  $(\alpha, \beta, \gamma) = (2, 2, 2), W_0 = 0.2$ , (b1), (b2)  $(\alpha, \beta, \gamma) = (2, 2, 2), W_0 = 0.5$ , (c1), (c2)  $(\alpha, \beta, \gamma) = (3, 2, 2), W_0 = 0.2$ , (d1), (d2)  $(\alpha, \beta, \gamma) = (3, 2, 1), W_0 = 0.2$ .

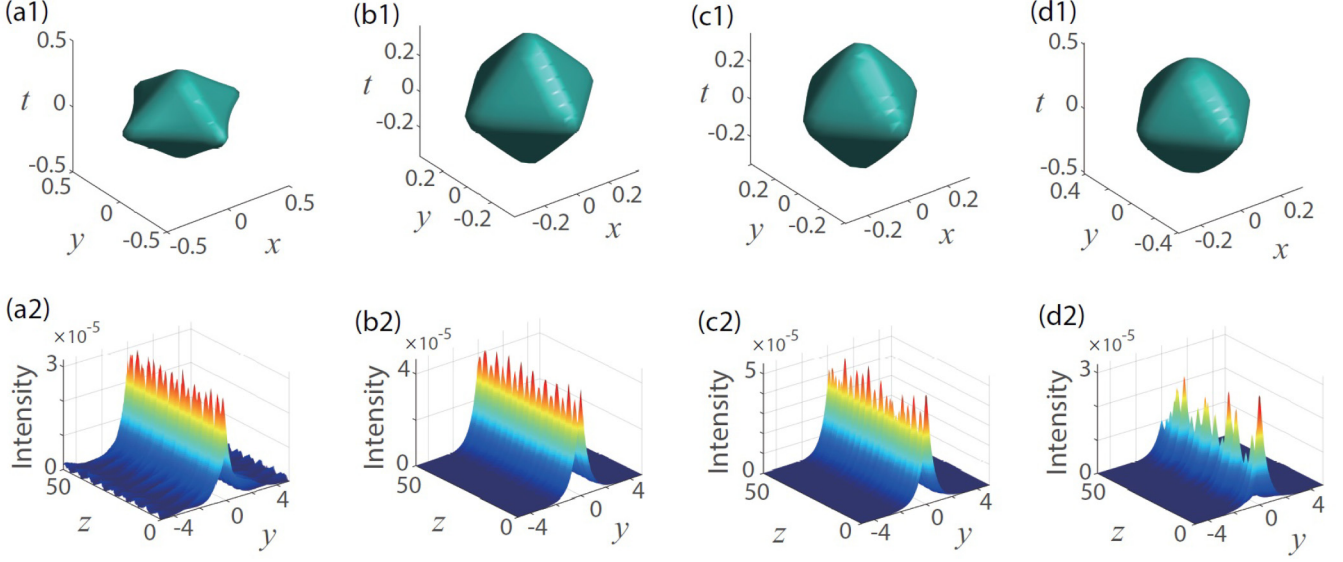


FIG. 9. Isosurface plots and propagation in the  $x = 0$  plane for numerically-acquired 3D peakons with: (a1), (a2)  $\mu = 3$ , (b1), (b2)  $\mu = 2$ , at  $(\alpha, \beta, \gamma) = (2, 2, 2)$ ; (c1), (c2)  $(\alpha, \beta, \gamma) = (3, 2, 2)$ ,  $\mu = 3$ , (d1), (d2)  $(\alpha, \beta, \gamma) = (3, 2, 1)$ ,  $\mu = 3$ . The common parameter is  $W_0 = 0.2$ .

ric DSE potential (24), likewise we can numerically capture stable peakons, as exhibited by Figs. 9(c1), 9(c2). However, with the loss of rotational symmetry, the propagation stability of the corresponding peakons will also get poor with dramatic periodic oscillation of the wave crest [see Figs. 9(d1), 9(d2)].

In a word, the 3D fundamental peakons can maintain stability in a certain range of potential parameters, no matter the exact or the numerical ones, the rotationally symmetric or the nonrotationally symmetric ones. Incompletely rotationally symmetric peakons can occur stably in completely rotationally symmetric DSE potentials. The stability of 3D peakons may get worse with the loss of rotational symmetry.

### B. EPs and peakons in $n$ dimensions

In the end, we will summarize the exact peakons in the  $n$ -dimensional DSE potential. For this purpose, we further generalize the  $\mathcal{PT}$ -symmetric DSE potential in the  $n$ -dimensional form

$$V(\mathbf{r}) = -\vec{\alpha} \cdot \vec{\delta}(\mathbf{r}),$$

$$W(\mathbf{r}) = W_0 \sum_{k=1}^n \alpha_k \operatorname{sgn}(x_k) e^{-\frac{1}{2}\alpha_k |x_k|}, \quad (29)$$

where  $\vec{\alpha} = (\alpha_1, \alpha_2, \dots, \alpha_n)$  and  $W_0$  are still all positive real-valued parameters modulating the complex-valued potential, and  $\vec{\delta}(\mathbf{r}) = [\delta(x_1), \delta(x_2), \dots, \delta(x_n)]$  is a real-valued vector function.

In the linear regime, it is not difficult to prove that the EPs  $\bar{W}_0(\vec{\alpha})$  of the  $n$ -dimensional  $\mathcal{PT}$ -symmetric Hamiltonian  $\mathcal{H} = -\Delta_{\mathbf{r}} + V(\mathbf{r}) + iW(\mathbf{r})$  given by the potential (29) obey the following relation, which is similar to that obtained in the 2D case:

$$\bar{W}_0(\vec{\alpha}) = \bar{W}_0[\min(\vec{\alpha})]. \quad (30)$$

It implies that the EPs in the  $n$ -dimensional space can also be converted to those in the corresponding 1D geometry.

If the spatially varying Kerr nonlinear coefficient grows exponentially as

$$g(\mathbf{r}) = \sum_{k=1}^n \exp(\sum_{j=1, j \neq k}^n \alpha_j |x_j|), \quad (31)$$

by means of the aforementioned analytical theory developed in Sec. III, we can readily obtain that Eq. (1) admits the exact solution of peakons having the following stationary-state form:

$$\psi(\mathbf{r}, z) = \frac{2}{3} W_0 \exp\left(-\frac{1}{2} \sum_{k=1}^n \alpha_k |x_k|\right) e^{i\varphi(\mathbf{r}) + i|\vec{\alpha}|^2 z/4} \quad (32)$$

with the phase function expressed as the second type of curve integral in the  $n$ -dimensional space

$$\varphi(\mathbf{r}) = -\frac{2W_0}{3} \int_0^{\mathbf{r}} \sum_{k=1}^n e^{-\frac{1}{2}\alpha_k |x_k|} dx_k. \quad (33)$$

### V. CONCLUSIONS AND DISCUSSIONS

To sum up, we have established a class of non-Hermitian  $\mathcal{PT}$ -symmetric DSE potentials in the  $n$ -dimensional geometry to expound the resulting peculiar exceptional-point phenomenon and peakon dynamics. First of all, through lots of numerical experiments, we observe that the EPs in the 2D DSE potential no matter rotationally symmetric or not can all boil down to those in the corresponding 1D potential in the linear regime, which is later confirmed by an analytical approach and further generalized to the  $n$ -dimensional case. In the presence of spatially varying Kerr nonlinearity, 2D analytical peakons are explicitly found, including the rotationally symmetric square peakons and the nonrotationally symmetric rhombic peakons. Both of them are proved to be stable within a specified parameter range. Around these stable exact peakons, one can additionally attain families of 2D stable peakons in internal modes by numerical methods. Adding the

adiabatic switches of potential parameters, different types of 2D peakons can be stably transformed to each other. Under spatial perturbations of external potentials, these 2D stable peakons can shift stably along the spatially changing potential well, which indicates that it is possible to control the propagation direction of the beam by adjusting the potential well wisely. Nevertheless, the 2D high-order peakons are usually susceptible to instability in propagation. Apart from that, 3D exact and numerical peakons are explored too. As a result, although the 3D fundamental peakons including the rotationally symmetric and the nonrotationally symmetric ones can keep stable in a certain range of potential parameters, their stability may become worse due to the loss of rotational symmetry. At last, we also present the explicit solution for the  $n$ -dimensional peakons.

Also, we need to emphasize that the theoretical ideas and numerical techniques developed in this paper can be expanded to other generalized nonlinear Schrödinger-like equations with alternative kinds of  $\mathcal{PT}$ -symmetric potentials, higher-order diffraction, and more complicated nonlinearities in the  $n$ -dimensional form as follows:

$$i \frac{\partial \psi}{\partial z} = H(\partial^q) \psi + \nabla^2 \psi + [V(\mathbf{r}) + iW(\mathbf{r})] \psi - g(\mathbf{r})N[\psi, \partial \psi, |\psi|^2, \partial(|\psi|^2), \dots], \quad (34)$$

where  $\psi \equiv \psi(\mathbf{r}, z)$  denotes the complex-valued wave function, noting that  $\partial^q = \partial_{x_1}^{q_1} \partial_{x_2}^{q_2} \dots \partial_{x_n}^{q_n}$ ,  $q$  is the nonnegative integer multiplicity index and  $|q| \geq 3$  is required here, thus  $H(\partial^q)$  stands for a high-order differential operator,  $g(\mathbf{r})$  is a real even function that depends on the spatial position; the complex potential  $V(\mathbf{r}) + iW(\mathbf{r})$ , the high-order differential operator  $H \equiv H(\partial^q)$  and the nonlinearity  $N \equiv N[\psi, \partial \psi, |\psi|^2, \partial(|\psi|^2), \dots]$  satisfy the  $\mathcal{PT}$  symmetry:  $V(-\mathbf{r}) = V(\mathbf{r})$ ,  $W(-\mathbf{r}) = -W(\mathbf{r})$ ,  $[\mathcal{PT}, H] = 0$ ,  $[\mathcal{PT}, N] = 0$ . It is fairly evident that the resulting nonlinear system (34) is indeed  $\mathcal{PT}$  invariant and involve the overwhelming majority of the common  $\mathcal{PT}$ -symmetric models. Moreover, one can examine the Poynting vector to confirm the direction of power flow and also explore the interaction between high-dimensional peakons.

Finally, the results reported in this paper may inspire the researchers to conceive and design new optical experiments, to synthesize other types of  $\mathcal{PT}$ -symmetric materials, and to offer some useful data to other underlying fields such as Bose-Einstein condensates.

#### ACKNOWLEDGMENTS

The work of Y.C. was supported by the National Natural Science Foundation of China under Grant No. 12001246. The work of Z.Y. was supported by the National Natural Science Foundation of China under Grant No. 11925108. The work of D.M. was supported by the Romanian Ministry of Research, Innovation, and Digitization under Grant No. PN 23210101/2023.

#### APPENDIX A: REPRESENTATION OF FUNDAMENTAL SOLUTIONS

In order to hunt for analytical soliton solutions of Eq. (10), we need beforehand to restrict the scope of exact solutions to the space of rapidly decreasing functions (alias Schwartz space), that is  $\phi(\mathbf{r}) \in \mathcal{S}(\mathbb{R}^n)$ , where

$$\mathcal{S}(\mathbb{R}^n) = \{f(\mathbf{r}) \in C^\infty(\mathbb{R}^n) \mid \lim_{|\mathbf{r}| \rightarrow \infty} \mathbf{r}^\alpha \partial^p f(\mathbf{r}) = 0, \\ \times \forall \alpha, p \in \mathbb{N}^n\},$$

$\mathbf{r}^\alpha \partial^p f(\mathbf{r}) \equiv x_1^{\alpha_1} \dots x_n^{\alpha_n} \partial_{x_1}^{p_1} \dots \partial_{x_n}^{p_n} f(\mathbf{r})$  and  $C^\infty(\mathbb{R}^n)$  denotes the space composed of infinitely continuous differentiable complex-valued functions on  $\mathbb{R}^n$ .

Without loss of generality, we assume  $\mu > 0$ . The Green's-function equation matched with Eq. (10) is

$$\nabla_{\mathbf{r}}^2 G - \mu G = \delta(\mathbf{r}) = \delta(x_1) \delta(x_2) \dots \delta(x_n). \quad (A1)$$

Making the Fourier transform and again its inverse transform on Eq. (A1) leads to the fundamental solution

$$G(\mathbf{r}) = -\frac{1}{(2\pi)^n} \int_{\mathbb{R}^n} \frac{e^{i\mathbf{r} \cdot \boldsymbol{\kappa}}}{|\boldsymbol{\kappa}|^2 + \mu} d\boldsymbol{\kappa}, \quad (A2)$$

then the analytical solution of Eq. (10) can be represented by a convolution in the following form:

$$\tilde{\phi} = G(\mathbf{r}) * [V(\mathbf{r})\phi + iW(\mathbf{r})\phi - g(\mathbf{r})|\phi|^2\phi]. \quad (A3)$$

It can be treated as a Bäcklund transformation formula of Eq. (10), from which we can immediately achieve another exact solution  $\tilde{\phi}$  theoretically only if a particular solution  $\phi$  is given. Thus the problem turns into how to seek for a series of particular nonlinear modes, among which are the most representative solitons.

More importantly, according to the formula (A3) and superposition principle, we can acquire more general solutions of Eq. (10) in a more specific form

$$\tilde{\phi} = C_1 \exp\left(\sum_{k=1}^n \gamma_k x_k\right) + C_2 \exp\left(\sum_{k=1}^{n-1} \gamma_k x_k - \gamma_n x_n\right) \\ + \int_{\mathbb{R}^n} G(\mathbf{r} - \mathbf{s}) [V(\mathbf{s})\phi(\mathbf{s}) + iW(\mathbf{s})\phi(\mathbf{s}) \\ - g(\mathbf{s})|\phi(\mathbf{s})|^2\phi(\mathbf{s})] ds. \quad (A4)$$

where  $\gamma_n = \sqrt{\mu - \sum_{k=1}^{n-1} \gamma_k^2}$  and  $C_1, C_2, \gamma_k (k = 1, 2, \dots, n-1)$  are all arbitrary constants. Particularly, in the 1D case, the formula (A4) turns to

$$\tilde{\phi}_1(x) = C_1 e^{\sqrt{\mu}x} + C_2 e^{-\sqrt{\mu}x} + \int_{\mathbb{R}} G(x - s) [V(s)\phi(s) \\ + iW(s)\phi(s) - g(s)|\phi(s)|^2\phi(s)] ds. \quad (A5)$$

As for the 2D setting, the formula (A4) reduces to

$$\tilde{\phi}_2(x, y) = C_1 e^{\gamma x + \sqrt{\mu - \gamma^2} y} + C_2 e^{\gamma x - \sqrt{\mu - \gamma^2} y} \\ + \int_{\mathbb{R}^2} G(x - s_1, y - s_2) [V(s_1, s_2)\phi(s_1, s_2) \\ + iW(s_1, s_2)\phi(s_1, s_2) \\ - g(s_1, s_2)|\phi(s_1, s_2)|^2\phi(s_1, s_2)] ds_1 ds_2. \quad (A6)$$

with  $\gamma$  being an arbitrary constant.

### APPENDIX B: NUMERICAL SCHEME OF NONLINEAR MODES

According to the spectral renormalization method [54], exerting the Fourier transform on Eq. (10) yields that

$$\hat{\phi}(\boldsymbol{\kappa}) = \frac{\mathcal{F}[g(\mathbf{r})|\phi|^2\phi] - \mathcal{F}[V(\mathbf{r})\phi] - i\mathcal{F}[W(\mathbf{r})\phi]}{|\boldsymbol{\kappa}|^2 + \mu}, \quad (\text{B1})$$

where the Fourier transform  $\mathcal{F}$  is defined by

$$\hat{\phi}(\boldsymbol{\kappa}) \equiv \mathcal{F}[\phi(\mathbf{r})] = \frac{1}{(\sqrt{2\pi})^n} \int_{\mathbb{R}^n} \phi(\mathbf{r}) e^{-i\mathbf{r}\cdot\boldsymbol{\kappa}} d\boldsymbol{\kappa}. \quad (\text{B2})$$

In order to converge the iterative scheme, a new field variable is usually drawn into, that is  $\phi(\mathbf{r}) = \tau \Phi(\mathbf{r})$ , thus  $\hat{\phi}(\boldsymbol{\kappa}) = \tau \hat{\Phi}(\boldsymbol{\kappa})$ , with  $\tau$  a nonzero constant to be determined. Then from

Eq. (B1) we have

$$\hat{\Phi} = \frac{\mathcal{F}[|\tau|^2 g(\mathbf{r})|\Phi|^2\Phi] - \mathcal{F}[V\Phi] - i\mathcal{F}[W\Phi]}{|\boldsymbol{\kappa}|^2 + \mu} \triangleq P_\tau(\boldsymbol{\kappa}). \quad (\text{B3})$$

Multiplying it by  $\hat{\Phi}^*(\boldsymbol{\kappa})$  and integrating over the entire  $\boldsymbol{\kappa}$  space goes to an equation with regard to  $\tau$  as follows:

$$\int_{\mathbb{R}^n} |\hat{\Phi}(\boldsymbol{\kappa})|^2 d\boldsymbol{\kappa} - \int_{\mathbb{R}^n} \hat{\Phi}^*(\boldsymbol{\kappa}) P_\tau(\boldsymbol{\kappa}) d\boldsymbol{\kappa} = 0. \quad (\text{B4})$$

As a consequence, the iteration scheme for achieving numerical nonlinear modes is

$$\hat{\Phi}_{l+1} = \frac{\mathcal{F}[|\tau_l|^2 g(r)|\Phi_l|^2\Phi_l] - \mathcal{F}[V\Phi_l] - i\mathcal{F}[W\Phi_l]}{|\boldsymbol{\kappa}|^2 + \mu}, \quad (\text{B5})$$

with  $\tau_l$  ( $l \in \mathbb{N}$ ) determined by

$$\int_{\mathbb{R}^n} |\hat{\Phi}_l(\boldsymbol{\kappa})|^2 d\boldsymbol{\kappa} - \int_{\mathbb{R}^n} \hat{\Phi}_l^*(\boldsymbol{\kappa}) P_{\tau_l}(\boldsymbol{\kappa})|_{\Phi=\Phi_l} d\boldsymbol{\kappa} = 0. \quad (\text{B6})$$

- 
- [1] C. M. Bender and S. Boettcher, Real spectra in non-Hermitian Hamiltonians having  $\mathcal{PT}$  symmetry, *Phys. Rev. Lett.* **80**, 5243 (1998).
- [2] Z. Musslimani, K. G. Makris, R. El-Ganainy, and D. N. Christodoulides, Optical solitons in PT periodic potentials, *Phys. Rev. Lett.* **100**, 030402 (2008).
- [3] Z. Shi, X. Jiang, X. Zhu, and H. Li, Bright spatial solitons in defocusing Kerr media with PT-symmetric potentials, *Phys. Rev. A* **84**, 053855 (2011).
- [4] S. Nixon, L. Ge, and J. Yang, Stability analysis for solitons in PT-symmetric optical lattices, *Phys. Rev. A* **85**, 023822 (2012).
- [5] V. Achilleos, P. Kevrekidis, D. Frantzeskakis, and R. Carretero-González, Dark solitons and vortices in PT-symmetric nonlinear media: From spontaneous symmetry breaking to nonlinear PT phase transitions, *Phys. Rev. A* **86**, 013808 (2012).
- [6] Z. Yan, Complex PT-symmetric nonlinear Schrödinger equation and Burgers equation, *Phil. Trans. R. Soc. A* **371**, 20120059 (2013).
- [7] Y. Lumer, Y. Plotnik, M. C. Rechtsman, and M. Segev, Nonlinearly induced PT transition in photonic systems, *Phys. Rev. Lett.* **111**, 263901 (2013).
- [8] Z. Yan, Z. Wen, and C. Hang, Spatial solitons and stability in self-focusing and defocusing Kerr nonlinear media with generalized parity-time-symmetric Scarff-II potentials, *Phys. Rev. E* **92**, 022913 (2015).
- [9] A. Guo, G. Salamo, D. Duchesne, R. Morandotti, M. Volatier-Ravat, V. Aimez, G. Siviloglou, and D. N. Christodoulides, Observation of PT-symmetry breaking in complex optical potentials, *Phys. Rev. Lett.* **103**, 093902 (2009).
- [10] C. E. Rüter, K. G. Makris, R. El-Ganainy, D. N. Christodoulides, M. Segev, and D. Kip, Observation of parity-time symmetry in optics, *Nature Phys.* **6**, 192 (2010).
- [11] A. Regensburger, C. Bersch, M.-A. Miri, G. Onishchukov, D. N. Christodoulides, and U. Peschel, Parity-time synthetic photonic lattices, *Nature (London)* **488**, 167 (2012).
- [12] G. Castaldi, S. Savoia, V. Galdi, A. Alù, and N. Engheta, PT metamaterials via complex-coordinate transformation optics, *Phys. Rev. Lett.* **110**, 173901 (2013).
- [13] A. Regensburger, M.-A. Miri, C. Bersch, J. Näger, G. Onishchukov, D. N. Christodoulides, and U. Peschel, Observation of defect states in PT-symmetric optical lattices, *Phys. Rev. Lett.* **110**, 223902 (2013).
- [14] B. Peng, S. K. Özdemir, F. Lei, F. Monifi, M. Gianfreda, G. L. Long, S. Fan, F. Nori, C. M. Bender, and L. Yang, Parity-time-symmetric whispering-gallery microcavities, *Nature Phys.* **10**, 394 (2014).
- [15] A. A. Zyablovsky, A. P. Vinogradov, A. A. Pukhov, A. V. Dorofeenko, and A. A. Lisyansky, PT-symmetry in optics, *Phys. Usp.* **57**, 1063 (2014).
- [16] P.-Y. Chen and J. Jung, PT symmetry and singularity-enhanced sensing based on photoexcited graphene metasurfaces, *Phys. Rev. Appl.* **5**, 064018 (2016).
- [17] K. Takata and M. Notomi, PT-symmetric coupled-resonator waveguide based on buried heterostructure nanocavities, *Phys. Rev. Appl.* **7**, 054023 (2017).
- [18] H. Hodaei, A. U. Hassan, S. Wittek, H. Garcia-Gracia, R. El-Ganainy, D. N. Christodoulides, and M. Khajavikhan, Enhanced sensitivity at higher-order exceptional points, *Nature (London)* **548**, 187 (2017).
- [19] B. Liu, H.-F. Zhang, R.-X. Zhong, X.-L. Zhang, X.-Z. Qin, C. Huang, Y.-Y. Li, and B. A. Malomed, Symmetry breaking of quantum droplets in a dual-core trap, *Phys. Rev. A* **99**, 053602 (2019).
- [20] A. Szenes, Exceptional points for Lebesgue's density theorem on the real line, *Adv. Math.* **226**, 764 (2011).
- [21] R. El-Ganainy, K. G. Makris, M. Khajavikhan, Z. H. Musslimani, S. Rotter, and D. N. Christodoulides, Non-Hermitian physics and PT symmetry, *Nature Phys.* **14**, 11 (2018).
- [22] J. Luo, J. Li, and Y. Lai, Electromagnetic impurity-immunity induced by parity-time symmetry, *Phys. Rev. X* **8**, 031035 (2018).
- [23] Ş. K. Özdemir, S. Rotter, F. Nori, and L. Yang, Parity-time symmetry and exceptional points in photonics, *Nature Mater.* **18**, 783 (2019).
- [24] M.-A. Miri and A. Alù, Exceptional points in optics and photonics, *Science* **363**, eaar7709 (2019).

- [25] E. A. Ultanir, G. I. Stegeman, and D. N. Christodoulides, Dissipative photonic lattice solitons, *Opt. Lett.* **29**, 845 (2004).
- [26] K. G. Makris, R. El-Ganainy, D. N. Christodoulides, and Z. H. Musslimani, Beam dynamics in PT symmetric optical lattices, *Phys. Rev. Lett.* **100**, 103904 (2008).
- [27] K. G. Makris, R. El-Ganainy, D. N. Christodoulides, and Z. H. Musslimani, PT-symmetric optical lattices, *Phys. Rev. A* **81**, 063807 (2010).
- [28] K. Makris, R. El-Ganainy, D. Christodoulides, and Z. H. Musslimani, PT-symmetric periodic optical potentials, *Int. J. Theor. Phys.* **50**, 1019 (2011).
- [29] Z. H. Musslimani, K. G. Makris, R. El-Ganainy, and D. N. Christodoulides, Analytical solutions to a class of nonlinear Schrödinger equations with PT-like potentials, *J. Phys. A* **41**, 244019 (2008).
- [30] S. Hu, X. Ma, D. Lu, Z. Yang, Y. Zheng, and W. Hu, Solitons supported by complex PT-symmetric Gaussian potentials, *Phys. Rev. A* **84**, 043818 (2011).
- [31] J. Yang, Symmetry breaking of solitons in one-dimensional parity-time-symmetric optical potentials, *Opt. Lett.* **39**, 5547 (2014).
- [32] D. A. Zezyulin and V. V. Konotop, Nonlinear modes in the harmonic PT-symmetric potential, *Phys. Rev. A* **85**, 043840 (2012).
- [33] C.-Q. Dai, X.-G. Wang, and G.-Q. Zhou, Stable light-bullet solutions in the harmonic and parity-time-symmetric potentials, *Phys. Rev. A* **89**, 013834 (2014).
- [34] B. Midya and R. Roychoudhury, Nonlinear localized modes in PT-symmetric Rosen-Morse potential wells, *Phys. Rev. A* **87**, 045803 (2013).
- [35] H. Cartarius and G. Wunner, Model of a PT-symmetric Bose-Einstein condensate in a  $\delta$ -function double-well potential, *Phys. Rev. A* **86**, 013612 (2012).
- [36] F. Single, H. Cartarius, G. Wunner, and J. Main, Coupling approach for the realization of a PT-symmetric potential for a Bose-Einstein condensate in a double well, *Phys. Rev. A* **90**, 042123 (2014).
- [37] C. P. Jisha, L. Devassy, A. Alberucci, and V. Kuriakose, Influence of the imaginary component of the photonic potential on the properties of solitons in PT-symmetric systems, *Phys. Rev. A* **90**, 043855 (2014).
- [38] F. K. Abdullaev, Y. V. Kartashov, V. V. Konotop, and D. A. Zezyulin, Solitons in  $\mathcal{PT}$ -symmetric nonlinear lattices, *Phys. Rev. A* **83**, 041805(R) (2011).
- [39] N. Moiseyev, Crossing rule for a PT-symmetric two-level time-periodic system, *Phys. Rev. A* **83**, 052125 (2011).
- [40] C. P. Jisha, A. Alberucci, V. A. Brazhnyi, and G. Assanto, Nonlocal gap solitons in PT-symmetric periodic potentials with defocusing nonlinearity, *Phys. Rev. A* **89**, 013812 (2014).
- [41] H. Wang and D. N. Christodoulides, Two dimensional gap solitons in self-defocusing media with PT-symmetric superlattice, *Commun. Nonlinear Sci. Numer. Simul.* **38**, 130 (2016).
- [42] I. Komis, S. Sardelis, Z. Musslimani, and K. Makris, Equal-intensity waves in non-Hermitian media, *Phys. Rev. E* **102**, 032203 (2020).
- [43] Z. Yan, Z. Wen, and V. V. Konotop, Solitons in a nonlinear Schrödinger equation with PT-symmetric potentials and inhomogeneous nonlinearity: Stability and excitation of nonlinear modes, *Phys. Rev. A* **92**, 023821 (2015).
- [44] S. V. Suchkov, A. A. Sukhorukov, J. Huang, S. V. Dmitriev, C. Lee, and Y. S. Kivshar, Nonlinear switching and solitons in PT-symmetric photonic systems, *Laser Photon. Rev.* **10**, 177 (2016).
- [45] G. Burlak and B. A. Malomed, Stability boundary and collisions of two-dimensional solitons in PT-symmetric couplers with the cubic-quintic nonlinearity, *Phys. Rev. E* **88**, 062904 (2013).
- [46] Y. V. Bludov, V. V. Konotop, and B. A. Malomed, Stable dark solitons in PT-symmetric dual-core waveguides, *Phys. Rev. A* **87**, 013816 (2013).
- [47] D. Dizdarevic, D. Dast, D. Haag, J. Main, H. Cartarius, and G. Wunner, Cusp bifurcation in the eigenvalue spectrum of PT-symmetric Bose-Einstein condensates, *Phys. Rev. A* **91**, 033636 (2015).
- [48] C.-Q. Dai, X.-F. Zhang, Y. Fan, and L. Chen, Localized modes of the  $(n + 1)$ -dimensional Schrödinger equation with power-law nonlinearities in PT-symmetric potentials, *Commun. Nonlinear Sci. Numer. Simul.* **43**, 239 (2017).
- [49] Z. Yan, Y. Chen, and Z. Wen, On stable solitons and interactions of the generalized Gross-Pitaevskii equation with PT-and non-PT-symmetric potentials, *Chaos* **26**, 083109 (2016).
- [50] V. V. Konotop, J. Yang, and D. A. Zezyulin, Nonlinear waves in PT-symmetric systems, *Rev. Mod. Phys.* **88**, 035002 (2016).
- [51] Y. He, B. A. Malomed, and D. Mihalache, Localized modes in dissipative lattice media: an overview, *Philos. T. R. Soc. A* **372**, 20140017 (2014).
- [52] D. N. Christodoulides and J. Yang, *Parity-time Symmetry and its Applications* (Springer, Berlin, 2018).
- [53] Y. Chen, Z. Yan, and D. Mihalache, Stable flat-top solitons and peakons in the PT-symmetric  $\delta$ -signum potentials and nonlinear media, *Chaos* **29**, 083108 (2019).
- [54] M. J. Ablowitz and Z. H. Musslimani, Spectral renormalization method for computing self-localized solutions to nonlinear systems, *Opt. Lett.* **30**, 2140 (2005).
- [55] J. Yang and T. I. Lakoba, Universally-convergent squared-operator iteration methods for solitary waves in general nonlinear wave equations, *Stud. Appl. Math.* **118**, 153 (2007).
- [56] J. Yang, Newton-conjugate-gradient methods for solitary wave computations, *J. Comput. Phys.* **228**, 7007 (2009).
- [57] J. Yang, *Nonlinear Waves in Integrable and Nonintegrable Systems* (SIAM, Philadelphia, 2010).
- [58] M. Zhong, Y. Chen, Z. Yan, and S. Tian, Formation, stability, and adiabatic excitation of peakons and double-hump solitons in parity-time-symmetric Dirac- $\delta(x)$ -Scarf-II optical potentials, *Phys. Rev. E* **105**, 014204 (2022).
- [59] B. A. Malomed, D. Mihalache, F. Wise, and L. Torner, Spatiotemporal optical solitons, *J. Opt. B* **7**, R53 (2005).
- [60] B. Malomed, L. Torner, F. Wise, and D. Mihalache, On multi-dimensional solitons and their legacy in contemporary atomic, molecular and optical physics, *J. Phys. B* **49**, 170502 (2016).
- [61] D. Mihalache, Localized structures in optical and matter-wave media: A selection of recent studies, *Rom. Rep. Phys.* **73**, 403 (2021).
- [62] B. A. Malomed, *Multidimensional Solitons* (AIP Publishing, New York, 2022).